

# When Flow Rates Matter: a dimensionless analysis of the effect of heat energy convection on microfluidic chip power consumption and temperature homogeneity

Brent C. Satterfield<sup>a</sup>, Jay A. A. West<sup>b</sup>, Michael R. Caplan<sup>\*a</sup>

<sup>a</sup>Harrington Department of Bioengineering, Arizona State University Tempe, AZ, USA

<sup>b</sup>Department of Microfluidics, Sandia National Laboratories-Livermore, CA, USA

\*Corresponding author: Michael R. Caplan, P.O. Box 879709, Tempe, AZ. Phone: 480-965-5144; Fax: 480-727-7624; E-mail: Michael.Caplan@asu.edu  
Current affiliation for Jay A. A. West: Arcxis Biotechnologies, Pleasanton, CA, USA.

**Abstract:** Portable biochips used in bioterror surveillance require low power heat transfer technologies in order to be battery operable. Here we derive and experimentally validate a dimensionless macroscopic energy balance relating dimensionless flow rate ( $\dot{m}_f cp_f h_{\text{eff}}^{-1} A^{-1}$ ), where  $\dot{m}_f$  is mass flow rate ( $\text{g min}^{-1}$ ),  $cp_f$  is heat capacity of fluid,  $h_{\text{eff}}$  is effective heat transfer coefficient, and  $A$  is surface area of the biochip, to dimensionless power consumption ( $\eta Q h_{\text{eff}}^{-1} A^{-1} \Delta T^{-1}$ ), where  $\eta$  is the device's heat transfer efficiency,  $Q$  is power supplied by the heat transfer device, and  $\Delta T$  is the temperature differential between the biochip and ambient air. At dimensionless flow rates less than 0.1, energy loss to the fluid is a negligible contribution to power consumption and chip temperature is homogenous. At dimensionless flow rate equal to 1.0, energy loss to the fluid accounts for half of the power consumption and power requirements.

## 1. INTRODUCTION

Defending against bioterrorism requires rapid, accurate, and portable methods of biological detection and identification. Microfluidic based sensors have great potential due to the ability to control flow and thermal dynamics and reduce diffusion distances to enable accurate and rapid detection of biological materials such as nucleic acids and proteins. In addition, such microfluidic chip-based platforms can be inexpensively mass produced and can be packaged to allow portability. Microfluidic microarrays for example have been developed to screen for a large number of biological agents in tandem [24]. However, unless designed for battery operation, these devices are useless in the field [8].

Limited previous work has been performed in modeling multiple aspects of the microchip environment using both fluid dynamics and heat transfer. Software modeling methods [14], heat transfer and fluid dynamic modeling of gases [4,7,10], liquids [1,5,6,11,22] phase changes [12,19] joule heating [9], and heat exchangers [13] have all been applied to the microfluidic environment. In addition, there is a plethora of work involving energy balances and the conversion of energy from one form to another in microfluidic systems. The majority of

energy analyses in microfluidic systems have been aimed at modeling microfluidics as a means of removing heat from microchips and microelectronics [16,21]. Another source of microfluidic energy balance is involved in the study of constant flow polymerase chain reaction (PCR) [15]. Sabry *et al.* recognized that traditional heat transfer models may not always apply and that the deviations from prediction increase as the size of the microfluidic channels decreases [18].

Erickson and Li observed that one of the most prominent obstacles in realizing the goal of portable microfluidic analysis is the limitation of standard batteries in supplying sufficient power to maintain adequate temperature control over the reaction chambers within a biochip [8]. Their models demonstrate the importance of material selection and the effect of increased power on transient time. They claim as much as 90% power reduction over standard methods. However, the model used by Erickson and Li is fairly specific to the heat transfer method and biochip setup proposed in their study and is not conducive to rational design of microfluidic chips in general. Further, Erickson and Li's model, while providing many insights, did not fully explore the ramifications of flow rate on

heat transfer device power requirements nor was it validated experimentally.

Here we design a model useful for rational design of low power microfluidic systems by determining the contribution of liquid convection to device power consumption and chip temperature variation. The model uses parameters that are readily measured or estimated in order to give a reasonable *a priori* calculation of the contribution of fluid flow rate to device power consumption. Due to the small volume of fluid relative to the overall volume of the biochip, it may seem reasonable to assume that the contribution of fluid convection to power consumption is negligible. However, we demonstrate that there is a threshold beyond which fluid flow rate becomes significant to power consumption. Additionally, flow rates exceeding this threshold were observed to produce large temperature gradients within the chip, disrupting one of the foundational assumptions in microfluidic diagnostics. This is extremely important since slight deviations in chip temperature can cause biochip failure in terms of expected molecular interactions and diagnostic accuracy. Our data indicate the model will allow rational design of devices, supporting platforms, and protocols for use of these which can accomplish reliable and rapid detection of biological agents.

## Theory

The principle of Conservation of Energy is applied to a microfluidic systems using the following ten simplifying assumptions [3,23]. The system is open. 2) No shaft work is done on or by the system as the biochip has no moving parts. 3) Heat generated by viscous losses is minimal. 4) The chip temperature has reached steady state. 5) Chip temperature is homogenous. Although we show below that this assumption is violated at high flow rates, the energy consumption due to fluid convection overwhelms energy consumption due to conduction from the chip so the equation maintains validity. This concept is analyzed in the Discussion section. 6) Radiant heat loss is negligible. 7) Heat loss to the ambient only occurs on sides not contacting the heat transfer device as shown in figure 1 (the arrow shows the combined conductive term  $h_{\text{eff}} A \Delta T_c$  leaving the system which would be the case for a heated chip). The heat transfer coefficient in this model is a lumped-parameter representing both conductive

losses to the manifold and the ambient air. 8) Heat is transferred into the chip only on the side contacting the heat transfer device ( $\eta Q$  in figure 1). While chip and subsequently fluid heating is the conventional goal, the model can also be modified to predict the effects of active cooling by reversing the signs adopted in this paper. 9) The energy transferred into the chip is proportional ( $\eta$ ) to the energy supplied to the heat transfer device. 10) The thermo-physical constants are constant with emperature [18]. These assumptions render the basic equation for the microchip heat balance as follows:

$$\eta Q = \dot{m}_f \Delta H_f + h_{\text{eff}} A \Delta T_c \quad (1)$$

where the term  $\eta Q$  represents energy entering the biochip from the TEC where  $\eta$  is the heat transfer device efficiency and  $Q$  is the power consumption of the device, and the term  $\dot{m}_f \Delta H_f$  represents the difference in energy entering and leaving the chip through fluid flow in the microfluidic channels, where  $\dot{m}_f$  is the mass flow rate of the fluid and  $\Delta H_f$  is the difference in enthalpy of the fluid. The final term,  $h_{\text{eff}} A \Delta T_c$ , represents heat loss to the ambient, where  $h_{\text{eff}}$  is the effective heat transfer coefficient,  $A$  is the area of the upper surface of the chip, and  $\Delta T_c$  is the temperature differential between the chip and the ambient. Figure 1 illustrates each heat transfer term in relation to the biochip open system.

The equation is then simplified further by substituting the product of the specific heat of the fluid ( $c_{p,f}$ ) and the temperature differential of the entering and exiting fluid ( $\Delta T_f$ ) for the enthalpy term ( $\Delta H_f$ ) and then dividing through by the ambient convection term ( $h_{\text{eff}} A \Delta T_c$ ). This yields a dimensionless equation that theoretically functions regardless of heat transfer device technology, flow rate, fluid or chip composition, chip size, convective properties or temperature differential as long as the above ten assumptions are valid. Since the entering fluid temperature is typically room temperature and biochips require homogenous reaction temperatures, a final assumption that the temperature differential between chip and ambient ( $\Delta T_c$ ) and the differential between

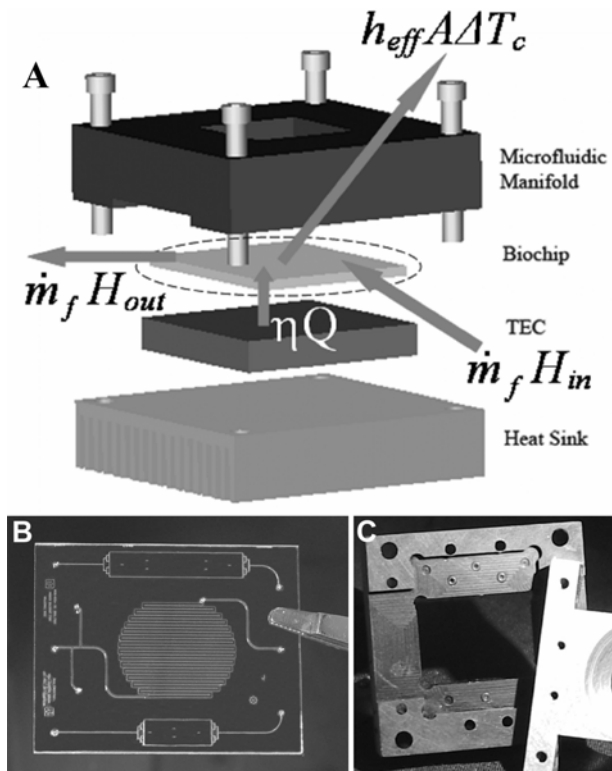


**Figure 1.** (A) Schematic diagram of heat transfer to/from biochip. Components from top to bottom include a microfluidic manifold, biochip, thermoelectric cooler (TEC), and heat sink. The three arrows correspond to the heat transfer into and out of the chip as written in equation (1). They correspond to heat loss to the ambient,  $h_{eff} A \Delta T_c$ , net liquid convective heat loss,  $\dot{m}_f (H_{out} - H_{in})$ , and heat transferred from the TEC into the chip,  $\eta Q$ . Arrows are drawn to represent the direction of heat transfer for a heated chip. Arrows would be in the opposite direction for a cooled chip. (B & C) Show chip and manifold respectively.

entering and exiting fluid ( $\Delta T_f$ ) is the same yields the following simplified equation:

$$\frac{\eta Q}{h_{eff} A \Delta T} = \dot{m}_f \left( \frac{c_{p,f}}{h_{eff} A} \right) + 1 \quad (2)$$

A quick analysis of the equation yields an understanding of the relationship between biochip parameters, specifically the fluid flow rate and energy requirements by the heat transfer device. It can be seen that the right hand side of the equation is the sum of the dimensionless flow rate ( $\dot{m}_f c_{pf} h_{eff}^{-1}$

$A^{-1}$ ), and one, which sum acts as a power multiplier. Thus, the dimensionless power ( $\eta Q h_{eff}^{-1} A^{-1} \Delta T^{-1}$ ) is at a minimum when the dimensionless flow rate approaches zero. A semi-log plot (figure 2) of the dimensionless power versus dimensionless flow rate shows this relationship graphically.

As the dimensionless flow rate goes to zero, the dimensionless power approaches its minimum at 1. Thus, dimensionless flow rates less than 0.1 should have nearly equivalent power consumption to no flow conditions. Flow rates yielding a dimensionless flow rate greater than 0.1 are predicted to have a significant impact on the power requirements of the device. For example, a dimensionless flow rate of 1.0 should cause the power consumption to double, and at flow rates greater than 1.0 dimensionless power consumption increases linearly as a function of the dimensionless flow rate.

## 2. MATERIALS AND METHODS

### Biochip Setup

A microfluidic microarray chip and supporting platform were designed and fabricated as shown in figure 1. Chips were fabricated from fused silica wafers. A 2.54 cm (width) by 3.18 cm (length) by 0.15 cm (thick) chip was designed to contain multiple channels for both target analyte concentration as well as deposition of genearrays in a 30 cm x 300  $\mu\text{m}$  x 20  $\mu\text{m}$  (LxWxD) microchannel (figure 1B). The open microchannels are sealed using a polymer film by either chemical bonding or compression to allow fluid flow through the microchannel. Sealed chips are mated to a manifold which provides an O-ring seal of the via-holes located on the microfluidic chip. In this arrangement a fused silica capillary (Polymicro Sciences, Phoenix, AZ) can be connected to the manifold through which fluids are pumped through the microchannel. The chip and a thermoelectric cooler (Marlow Industries, Dallas, Texas) are sandwiched between a standard computer heat sink (4.45 cm x 4.45 cm x 1.27 cm) and the manifold to complete assembly.

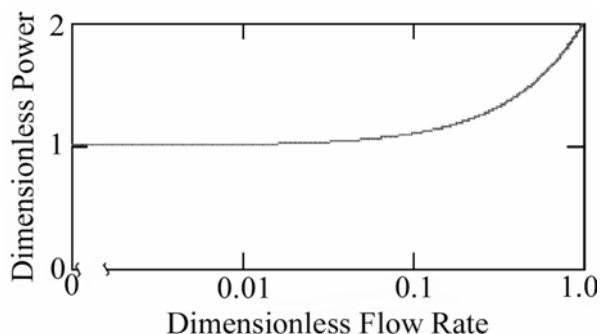


**Figure 2.** Semi-log plot of model results showing the relationship between dimensionless power ( $\eta Q h_{\text{eff}}^{-1} A^{-1} \Delta T^{-1}$ ) and dimensionless flow rate ( $\dot{m}_f c_{p,f} h_{\text{eff}}^{-1} A^{-1}$ ).

Convection does not add appreciably to power consumption at dimensionless flow rates less than 0.1. At dimensionless flow rate equal to 1.0, the dimensionless power consumption doubles and continues to increase linearly as a function of the dimensionless flow rate.

## 2.2 Dimensionless Flow Rate Determination

Initial estimates were made of the flow rates necessary to obtain the required dimensionless flow rates. Mass flow rate ( $m_f$ ) was related to the volumetric flow rate by the density of the fluid, in this case water  $\rho = 1.0 \text{ g cm}^{-3}$  [23]. We used flow rates near  $0 \mu\text{L min}^{-1}$ ,  $1.0 \mu\text{L min}^{-1}$ ,  $10 \mu\text{L min}^{-1}$ ,  $100 \mu\text{L min}^{-1}$ , and  $1.0 \text{ mL min}^{-1}$  in order to obtain dimensionless flow rate values of approximately 0, 0.001, 0.01, 0.1, and 1.0.

The flow rates were measured by using a stop watch and an automated syringe pump. A 1 mL syringe (10 mL syringe for the  $1.0 \text{ mL min}^{-1}$  case) was loaded with Milli-Q water and the flow rate was calculated by dividing the volume of fluid pumped by the time elapsed. The initial flow rate was determined to be  $103 \mu\text{L min}^{-1}$ . The flow rates were altered by magnitudes of 10 by increasing or decreasing the automated pump rate by a factor of 10.

## 2.3 Measurements

The power consumption of the thermo-electric cooler (TEC) was determined at various flow rates. First, a variable power supply was attached to the TEC, then a voltmeter was placed in parallel with the TEC and an ammeter in series with it.

The ambient temperature was measured with a K-type thermocouple and checked against a standard

thermometer for accuracy. The K-type thermocouple was used to detect the temperature of the biochip throughout the rest of the experiment. In order to perform the experiment, the thermocouple was secured to the location on the chip nearest the exit of the fluid channel. The fluid flow was started at the appropriate flow rate and the variable power supply was adjusted until the chip temperature reached and maintained a steady state value of  $60 \text{ }^\circ\text{C} \pm 0.5 \text{ }^\circ\text{C}$  for 30 s. The current and voltage were then recorded.

The experimental order was randomized and three replicates were performed at each flow rate by first allowing the biochip to cool and then repeating the experiment. The power consumption was determined by multiplying the voltage drop by the current for each trial. An average power consumption ( $Q$ ) was then found for each of the flow rates.

## 2.4 Statistics

The best fit values of  $h_{\text{eff}}$  and  $\eta$  were used with the values for each of the other parameters in equation (2) to calculate the actual dimensionless flow rate and dimensionless power. The dimensionless power was calculated from the average power at each flow rate. These values were then input into Minitab statistical software and analyzed for regression. By choosing the fitted equation feature, Minitab automatically computed the slope and intercept of the data using sum of the least square errors and gave corresponding 95% confidence intervals. The regression coefficient was also given, displaying the quality of the fit. The fitted equation with 95% confidence intervals was then compared to equation (2). In order to compare the model to the fitted data statistically, a two-step t-test was used. The first t-test compared the fitted slope with the theoretical slope of one. The second t-test compared the experimentally determined intercept with the analytically derived intercept of one. The number of samples used for calculation in the t-tests was equal to the number of data points taken. The decision criteria used was 95% confidence ( $p < 0.05$ ).

### 3. RESULTS

The voltages and currents with their corresponding calculated powers are recorded in Table 1. Power was computed by  $V \cdot I = P$ , where  $V$  is voltage,  $I$  is current, and  $P$  is power. The experimental values of power shown in Table 1 were used to compute the actual values of the heat transfer coefficient ( $h_{\text{eff}}$ ) and the efficiency ( $\eta$ ) by minimizing the sum of the squared errors between experimental data ( $Q$ ) and model calculations ( $[\dot{m}_f c_{p,f} \Delta T + h_{\text{eff}} A \Delta T] / \eta$ ). The calculated surface area for this experiment was  $1.2 \times 10^{-3} \text{ m}^2$  for the five sides of the biochip not touching the TEC. The temperature differential was 36 K, the specific heat of water is  $4.179 \text{ J g}^{-1} \text{ K}^{-1}$  [23]. Using these values,  $h_{\text{eff}}$  and  $\eta$  were calculated as  $52.188 \text{ W m}^{-2} \text{ K}^{-1}$  and 0.73 respectively.

Flow Rate ( $\mu\text{L}/\text{min}$ )	Trial 1			Trial 2			Trial 3			Avg. P (W)
	V (V)	I (A)	P (W)	V (V)	I (A)	P (W)	V (V)	I (A)	P (W)	
0.00	4.99	0.49	2.45	4.77	0.47	2.24	5.25	0.50	2.63	2.44
1.03	5.38	0.51	2.74	5.67	0.56	3.29	5.49	0.52	2.85	2.96
10.34	6.32	0.59	3.73	6.12	0.58	3.55	5.78	0.55	3.18	3.49
103.40	6.31	0.60	3.79	6.10	0.58	3.54	6.03	0.58	3.50	3.61
1034.00	8.35	0.80	6.68	8.04	0.78	6.27	8.91	0.80	7.13	6.69

**Table 1.** Voltage ( $V$ ), current ( $I$ ), and power consumption ( $P$ ) at each flow rate. Three trials for each experimental condition were performed. A final column contains power averages for each flow rate.

These values of  $h_{\text{eff}}$  and  $\eta$  were used to calculate the dimensionless power for each of the flow rate values in Table 1, in addition to calculating the dimensionless flow rate. The results were plotted against the theoretical predictions (figure 3). Next, the data was examined for statistical relevance. The model generates a straight line (figure 3 is a semi-log plot causing a curved appearance), so statistical regression is both straightforward and relevant. The regression equation is

$$\frac{\eta Q}{h_{\text{eff}} A \Delta T} = 1.04 \dot{m}_f \left( \frac{c_{p,f}}{h_{\text{eff}} A} \right) + 0.975 \quad (3)$$

The above equation can be seen to be virtually identical to equation (2). The confidence intervals for the slope,  $1.04 \pm 0.1416$ , and for the intercept,  $0.975 \pm 0.07309$ , show that equation (3) is statistically identical to equation (2). The t-test for the slope had a p-value of 0.771, and the t-test for

the intercept had a p-value of 0.740. The residual for the fitted line is  $R^2 = 0.947$ .

### 4. DISCUSSION

Statistical evidence indicates that the model functions within adequate margins in order to predict the influence of flow rate on power consumption if  $h_{\text{eff}}$  and  $\eta$  are known. Provided the assumptions hold true and that there is a reasonable correlation between theoretical and fitted values for efficiency and the heat transfer coefficient, the model should serve to allow rational design of biochip parameters in order to minimize power consumption.

First, we examine the assumption of temperature homogeneity. As was expected, the temperature of the biochip was not entirely homogenous. However, the degree of nonhomogeneity far exceeded biochip requirements for stable reaction temperatures. During trials with higher flow rates (e.g.  $1 \text{ mL min}^{-1}$ ) the thermocouple reading at the exit of the channel was  $60^\circ \text{C}$  when other parts of the chip were up to 10-15 degrees warmer. The variation in chip temperature was much less for the biochip tested under low-flow conditions, varying by  $\pm 1.5^\circ \text{C}$ . This is extremely significant because of the importance of maintaining constant temperatures in biochips for diagnostic functionality and accuracy.

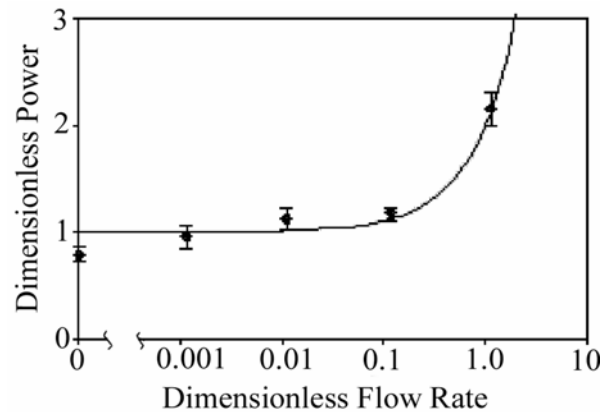


**Figure 3.** Model validation. This plot shows the model prediction (line) and experimental values (diamonds) of dimensionless power ( $\eta Q h_{\text{eff}}^{-1} A^{-1} \Delta T$ ) versus dimensionless flow rate ( $\dot{m}_f c_{p,f} h_{\text{eff}}^{-1} A^{-1}$ ). The error bars represent 95% confidence intervals.

It is also significant to note that this large increase in variation in chip temperature occurred when dimensionless flow rates exceeded the same threshold as was indicated for significance to power consumption (about 0.1). However, before entering into a more thorough discussion of this matter, we wish to address the effect this finding has on the assumptions and model validity.

The two assumptions of chip temperature homogeneity and of equal chip and fluid temperature differentials from the ambient are sufficiently satisfied for model functionality for two reasons: 1) The exiting fluid temperature is representative of the average chip temperature under high flow rates, being higher than the temperature of the chip contacting the entering fluid and lower than portions of the chip not near the fluid. 2) The error introduced to the model by these assumptions is small. The size of the error is decreased by the fact that at high flow rates, at which the chip begins to have substantial temperature gradients, the fluid is responsible for the majority of heat transfer as demonstrated by equation (2) and as graphically depicted in Figure 2. This diminishes the error introduced by increased chip temperature variability to acceptable levels. For example, if the temperature of the entire chip were 15 °C greater than the exiting fluid temperature of 60 °C at flow rates of 1 mL/min, the error in predicted power consumption would only amount to 20%

(Error =  $[hA(\Delta T_{\text{actual}} - \Delta T_{\text{predicted}})] / (\dot{m}_f c_{p,f} + hA\Delta T_{\text{actual}})$ ). Further, this 20% error only applies to estimates for biochips with very high dimensionless flow rates. Low or no-flow conditions (i.e.,  $< 1 \text{ mL min}^{-1}$ ) produce less variability in the chip surface temperature, thus less error. With respect to the temperature variation under no flow conditions, a temperature variation of  $\pm 1.5 \text{ }^\circ\text{C}$  correlates to a maximum error of 4.2% in predicted power consumption (Error =  $(\Delta T_{\text{actual}} - \Delta T_{\text{predicted}}) / \Delta T_{\text{actual}}$ ). Thus, while homogeneity in chip temperature may not be exact, it renders approximations within a satisfactory margin of error for rational design.

Perhaps the most significant result of the discovery of large temperature gradients within the chip at high dimensionless flow rates is its effect on the chemical reactions taking place in most sensors. Most biochips require uniform temperatures for hybridization assays, PCR or other applications. Even small variations in the temperature can produce unexpected and unreliable results. While the

model itself is not designed to predict when flow rates will cause large temperature variation, it is intuitive that large dimensionless flow rates, causing a significant increase in power consumption will also cause an increase in temperature variation of the chip. The data from this experiment shows that this is true for the biochip used in the experiment (figure 1B), producing temperature gradients in excess of  $\pm 1.5 \text{ }^\circ\text{C}$  for flow rates less than dimensionless flow rate of 0.1 and temperature gradients of  $\pm 15 \text{ }^\circ\text{C}$  for dimensionless flow rates greater than one. It is reasonable to assume similar results will occur for biochips of similar size and channel arrangement. While low dimensionless flow rates are no guarantee of temperature uniformity, high dimensionless flow rates appear to be a good indicator of the lack thereof.

Next we evaluate the correlation between theoretical and experimental values of  $\eta$  and  $h_{\text{eff}}$  for purposes of rational design. In this study, we best fit values for two parameters,  $\eta$  and  $h_{\text{eff}}$ ; however, for rational design we show how values for these parameters could have been estimated with no experimental effort required. Efficiencies of thermoelectric coolers generally fall between values of 0.3 and 0.7 [20], which compare reasonably well to the best fit value of 0.73. However, the efficiency constant is used to calculate dimensionless power, which is necessary only to demonstrate model validity. Thus, for rational design only the independent variable, the dimensionless flow rate ( $\dot{m}_f c_{p,f} h_{\text{eff}}^{-1} \text{ A}^{-1}$ ), is needed. Therefore  $h_{\text{eff}}$  alone requires approximation.

Since the specific heat of the fluid is constant and the biochip surface area and flow rates are determined by designers, the only other necessary parameter to determine is the heat transfer coefficient. Estimates for rational design can be made by creating a weighted average for ambient heat loss and conduction. For Rayleigh number (a dimensionless number relating conduction to convection) greater than 10 [10] and less than 10 [5], the equation for free convection is [2]:

$$h = \frac{2(0.54)k}{L} \left[ \left( \frac{Ra}{L^3 \Delta T} \right) (L^3 \Delta T) \right]^{1/4} \quad (4)$$

where  $Ra$  is the average Rayleigh Number,  $\Delta T$  is the temperature difference between the chip and the ambient,  $L$  is the characteristic length which is the average length of the two sides of the biochip, and  $k$  is the thermal conductivity of the biochip. All of these inputs can be determined with no experimentation to provide an estimate for the heat transfer coefficient ( $h$ ) of air. Air at room temperature has a Rayleigh number divided by the characteristic length cubed and the temperature differential,  $Ra/(L^3\Delta T)$ , of  $90.7 \text{ cm}^{-3} \text{ K}^{-1}$  [2]. Silica has a thermal conductivity of  $1.4 \text{ W m}^{-1} \text{ K}^{-1}$ , the characteristic length is 2.86 cm, the temperature differential is 36 K and the Rayleigh number is computed as 60195 ( $Ra = 90.7 \text{ cm}^{-3} \text{ K}^{-1} \times L^3\Delta T$ ), which justifies the use of equation (4). Using these values, the natural convection portion of the heat transfer coefficient is calculated as  $8.79 \text{ W m}^{-2} \text{ K}^{-1}$ .

The manifold is made of polyetheretherketone (PEEK) which has conduction values ranging from 0.25 to  $0.92 \text{ W m}^{-1} \text{ K}^{-1}$ , depending on the method of manufacture [17]. Using an average value of  $0.585 \text{ W m}^{-1} \text{ K}^{-1}$  and considering the 1 cm thickness of the manifold, the conduction per unit length, the conduction portion of the heat transfer coefficient, is rendered  $58.5 \text{ W m}^{-2} \text{ K}^{-1}$ .

In order to form the weighted average, the proportions of surface area involved in free convection and conduction must be calculated. Neglecting the sides of the biochip, which are small and whose contribution is assumed negligible in order to simplify this calculation, the surface area in contact with air is  $2.72 \text{ cm}^2$  and the conductive surface area in contact with the manifold is  $5.34 \text{ cm}^2$ , while the total surface area of the upper surface of the biochip is  $8.06 \text{ cm}^2$ . This renders the ratio of natural convective surface area to the total surface area 0.338 and the ratio of the conductive surface area to the total surface area 0.662. The combined heat transfer coefficient ( $h_{\text{eff}}$ ) is therefore  $41.7 \text{ W m}^{-2} \text{ K}^{-1}$ . This number compares well with the experimental value of  $52.2 \text{ W m}^{-2} \text{ K}^{-1}$  and demonstrates the feasibility of rational design. For a dimensionless flow rate of one at which dimensionless power is doubled the estimated mass flow rate is  $718 \mu\text{L min}^{-1}$ , compared to an actual mass flow rate of  $899 \mu\text{L min}^{-1}$ . This yields a 20% error in prediction for the biochip studied.

## 5. CONCLUSION

Biosensors are only field operable if they are battery operable. In this study we derive a dimensionless equation for rational design of low power biosensors relating dimensionless power consumption and dimensionless flow rate. We have shown how parameters for this equation can be estimated a priori with reasonable accuracy (within 20% error), and we have validated the model for an actual microfluidic device. We have demonstrated that microfluidic flow rates can have a significant impact on power consumption. We have further observed that microfluidic flow rates which result in significant power consumption are also likely to cause temperature inhomogeneity, leading to additional problems in hybridization and other assays.

## ACKNOWLEDGMENTS

We would like to thank Eric Guilbeau and Elena Rosca from Arizona State University for helpful discussion. We would further like to acknowledge Gary Hux and Kyle Hukari from Sandia National Laboratories for helpful assistance with laboratory equipment (biochip setup and biochip temperature controller). M.R.C. is funded by the National Institute of Dental and Craniofacial Research Career Development and Faculty Transition Award (K22 DE014846). B.C.S. performed this research while on appointment as a U.S. Department of Homeland Security (DHS) Fellow under the DHS Scholarship and Fellowship Program, a program administered by the Oak Ridge Institute for Science and Education (ORISE) for DHS through an interagency agreement with the U.S. Department of Energy (DOE). ORISE is managed by Oak Ridge Associated Universities under DOE contract number DE-AC05-00OR22750. All opinions expressed in this paper are the authors' and do not necessarily reflect the policies and views of DHS, DOE, or ORISE.

## REFERENCES

1. Ahmadi G. Special theories of heat-conducting microfluids. Bulletin de

- l'Academie Polonaise des Sciences, Serie des Sciences Techniques 1973;27(1):69-80.
2. Bejan A. Convective Heat Transfer. New Jersey: John Wiley & Sons; 2004.
  3. Bird RB, Stewart WE, Lightfoot EN. Transport Phenomena. New York: John Wiley & Sons, Inc; 1960.
  4. Chen K, Wu Y-E. Thermal analysis and simulation of the microchannel flow in miniature thermal conductivity detectors. Sensors and Actuators 2000;A79(3):211-218.
  5. Damean N, Regtien PPL, Elwenspoek M. Heat transfer in a MEMS for microfluidics. Sensors and Actuators 2003;A105(2):137-149.
  6. Deka RK, Soundalgekar VM. Heat transfer in a micropolar fluid through a porous medium with variable plate temperature. Journal of the Chinese Institute of Chemical Engineers 2003;34(4):493-496.
  7. Dillner U, Kessler E, Poser S, Baier V, Muller J. Thermal simulation of a micromachined thermopile-based thin-film gas flow sensor. Microelectronics journal 1998;29(4-5):291-297.
  8. Erickson D, Li D. Numerical simulations of a low power microchannel thermal cycling reactor. International journal of heat and mass transfer 2002;45(18):3759-3770.
  9. Erickson D, Sinton D, Li D. Joule heating and heat transfer in poly(dimethylsiloxane) microfluidic systems. Lab Chip 2003; 3(3):141-9.
  10. Fang Y, Liou WW. Computations of the flow and heat transfer in microdevices using DSMC with implicit boundary conditions. Journal of Heat Transfer 2002;124(2):338-345.
  11. Lao AIK, Lee TMH, Hsing I-M, Ip NY. Precise temperature control of microfluidic chamber for gas and liquid phase reactions. Sensors and Actuators 2000;A84(1-2):11-17.
  12. Peles YP, Yarin LP, Hetsroni G. Thermohydrodynamic characteristics of two-phase flow in a heated capillary. International Journal of Multiphase Flow 2000;26(7):1063-1093.
  13. Peterson RB. Numerical modeling of conduction effects in microscale counter-flow heat exchangers. Microscale Thermo-physical Engineering 1999;3(1):17-30.
  14. Przekwas A, Makhijani V, Athavale M, Klein A, Bartsch P. Computational simulation of bio-microfluidic processes in integrated DNA biochips. In: Van den Berg A, Olthuis W, Bergveld P, editors. Micro Total Analysis Systems 2000, Proceedings of the uTAS Symposium. Enschede, Netherlands: Kluwer Academic Publishers; 2000. p 561-564.
  15. Punch J, Rodgers B, Newport D, Davies M. Thermal analysis of a micro-polymerase chain reaction device. Proceedings of the ASME Heat Transfer Division 2004;1:667-674.
  16. Qu W, Mala GM, Li D. Heat transfer for water flow in trapezoidal silicon microchannels. International Journal of Heat and Mass Transfer 2002;43:3925-3936.
  17. Quadrant Engineering Plastic Products. Ketron® PEEK CA30 Polyetheretherketone, 30% carbon fiber reinforced, extruded. 2004.  
<http://www.quadrantepp.matweb.com/SpecificMaterialNew.asp?bassnum=P1SM17A&group=General>
  18. Sabry MN, Djebedjian BO, Saleh SH, Mahgoub MM. Modeling heat transfer and liquid flow in micro-channels. In: Ernst LJ, editor. International Conference on Thermal and Mechanical Simulation and Experiments in Microelectronics and Microsystems, Proceedings, 5th. Brussels, Belgium: New York: IEEE; 2004. p 511-518.
  19. Song YJ, Zhao TS. Modelling and test of a thermally-driven phase-change non-mechanical micropump. Journal of Micromechanics and Microengineering 2001;11(6):713-719.
  20. TE Technologies, Inc. Frequently Asked Questions on Thermoelectrics. 2005.  
<http://www.tetech.com/techinfo/#5>.
  21. Toh KC, Chen XY, Chai JC. Numerical computation of fluid flow and heat transfer in microchannels. International Journal of Heat and Mass Transfer 2002;45:5133-5141.
  22. Wang W, Li Z-X, Guo Z-Y. Numerical simulation on micro flow-through PCR chip. In: Kandlikar SG, editor. International Conference on Microchannels and Minichannels, 1st. Rochester, NY, United States: American Society of Mechanical Engineers; 2003. p 425-431.
  23. Welty JR, Wicks CE, Wilson RE, Rorrer G. Fundamentals of Momentum, Heat, and

- Mass Transfer. New York: John Wiley & Sons, Inc.; 2001.
24. West JAA, Hukari KW, Hux G, Shepodd TJ. Microfluidic gene arrays for rapid genomic profiling. In: Smith L, Sobek D, editors. Proceedings of the Society of Photo-Optical Instrumentation Engineers Conference on Lab-on-a-Chip: Platforms, Devices, and Applications. Volume 5591. Philadelphia, PA: Society of Photo-Optical Instrumentation Engineers; 2004. p 167-173.